electronics

MDPI

Article

Enhancement of Electromagnetic Scattering Computation Acceleration Using LSTM Neural Networks

Yuanpeng Yang [1], Shi Xinyang [2], Qingyao Wang [1] and Chonghua Fang [1,*]

[1] Science and Technology on Electromagnetic Compatibility Laboratory, China Ship Development and Design Centre, Wuhan 430060, China; wxhzkn0028@gmail.com (Y.Y.); q1941732362@gmail.com (Q.W.)
[2] Wuhan Maritime Communication Research Institute, Wuhan 430205, China; bourn80lee@gmail.com
* Correspondence: game6021023@gmail.com

Abstract: This paper presents the electromagnetic long short-term memory neural network (EM-LSTMNN) approach to accelerate radar cross-section (RCS) calculations in optimizing low RCS for electrically large targets. The proposed method converts the conventional electromagnetic numerical calculation into an efficient numerical calculation using the LSTM neural network, resulting in a significant improvement in RCS computation speed. To assess the effectiveness of this approach, a downscaled model of a large-sized ship is employed as the target for low RCS optimization. Each modification made to the target's mesh data during the optimization process is stored in the dataset as a new element. As the ship scaling model undergoes modifications during the optimization process, the new mesh data are recorded, thus adding a new element to the dataset at each time step. This forms a time series representation of the mesh model. By utilizing the dataset collected throughout the optimization process, the proposed EM-LSTMNN model is trained using data-driven approaches, with a training time of approximately 106 s. It is worth noting that this training time is significantly smaller compared to existing methods that employ fully connected neural networks. The performance of the proposed approach is demonstrated by comparing the RCS calculation results obtained through this method with those obtained through traditional electromagnetic simulations.

Keywords: full connected neural networks; long short-term memory neural network; time series data; electrically large targets; parameter optimization

check for updates

Citation: Yang, Y.; Xinyang, S.; Wang, Q.; Fang, C. Enhancement of Electromagnetic Scattering Computation Acceleration Using LSTM Neural Networks. *Electronics* **2023**, *12*, 3900. https://doi.org/10.3390/electronics12183900

Academic Editor: Gerardo Di Martino

Received: 14 August 2023
Revised: 12 September 2023
Accepted: 14 September 2023
Published: 15 September 2023

Copyright: © 2023 by the authors. Licensee MDPI, Basel, Switzerland. This article is an open access article distributed under the terms and conditions of the Creative Commons Attribution (CC BY) license (https://creativecommons.org/licenses/by/4.0/).

1. Introduction

The calculation of radar scattering characteristics for target objects is a significant research area in computational electromagnetics with great practical value. Traditional electromagnetic simulations and computing techniques have seen gradual advancements over the years, and several recent technologies combining traditional electromagnetic computing techniques have also emerged. With the progress in neural network research, utilizing neural networks to enhance traditional electromagnetic simulation methods has become a promising research direction.

Low RCS optimization is a crucial aspect of designing electrically large targets, such as ships. While computational electromagnetics has made significant advancements over the years, the computational speed of calculating RCS for the electrically large targets has greatly improved [1–14]. Existing methods that utilize neural networks for electromagnetic calculations have varying applicability. Some methods are suitable for calculating scattering in two-dimensional targets [1], while others rely on current source parameters [2]. Certain methods focus on radar signal processing [3,4]. Although these methods are useful for calculating scattering in small electric targets, they encounter difficulties when applied to RCS calculations for the electrically large targets [5–11,13]. The EM-FCNN method can be used for calculating the RCS of electrically large targets; however, it requires suitable physical prior data during neural network training and the acquisition of the input model's

point cloud matrix [12]. This increases the difficulty of applying this method to a low-RCS optimization process for electrically large targets. During the low-RCS optimization process of electrically large-sized targets, a significant amount of time is still required to continuously adjust the target model and simulate and calculate its RCS value [15,16]. When accelerating the electromagnetic simulation calculation of electrically large-sized targets with the help of neural networks, although previous studies provide feasible methods such as EM-FCNN, the neural network structure used in the low-RCS optimization process is still a general FCNN [12]. Recurrent neural networks with more complex structures have not been directly applied to calculate electromagnetic scattering problems, and the construction of EM-LSTMNN for RCS calculation in the optimization process of electrically large-size targets is a new application orientation. The EM-LSTMNN proposed in this paper obviates the requirement for extra computation of the point cloud matrix for the model. It utilizes the grid data of the model as input for the neural network directly, lessening the data processing steps in the low-RCS optimization process.

The chosen target in this study is an electrically large-scale model of a ship [17]. During the process of optimizing the target with a low RCS, it is necessary to make several modifications to the outer surface structure of the target's superstructure. Additionally, the grid data of the large-scale target need to be constantly changed during the optimization process. Storing the 3D mesh data of the electrically large target as an element allows for the creation of a time series composed of grids, as each adjustment to the target shape in the optimization process generates a new element. These new elements are arranged in the order of the optimization process. Since there are usually a large number of modifications during the optimization process, it aligns with the advantageous features of LSTM networks for processing long time series data. This paper posits that enhancing the network structure of the EM-FCNN network through the principles of LSTM can lead to an improved neural network. It can enhance the computing ability and accuracy of the improved neural network compared to the FCNN during the optimization process using time series data. In order to enhance the efficiency of low-RCS optimization design and reduce simulation calculation time, it is important to choose a neural network structure that is better suited for calculating the RCS of large electrical targets. This selection can significantly improve the calculation speed for large-sized electric targets, thereby increasing the overall optimization efficiency.

2. Literature Review

In the context of the forward scatter problem, Li Maokun et al. have explored the feasibility of neural networks for improving the iterative process in the volume integral equation [1]. Z. Wei et al. have contributed to solving the full-wave inverse scattering problem in electromagnetic computing using neural networks [2]. Yongmei Qi et al. have applied fully connected neural networks (FCNN) to process clutter in radar signals, reducing the target loss rate and minimizing errors caused by clutter when calculating the radar scattering cross-sectional area [3]. Josiah W. Smith has employed FCNN in mmWave radar, presenting novel FCNN-based super-resolution and tracking algorithms that offer an elegant solution to fine motion tracking problems [4].

Apart from FCNN, LSTM neural networks have found various applications in the field of electromagnetic technology. H. M. Yao et al. have used a long short-term memory (LSTM) network to replace the absorption boundary in electromagnetic simulation calculations [5]. Wenxiu Sima et al. have made notable contributions by utilizing the LSTM neural network in combination with deep residual networks to solve electromagnetic transient problems through small sample measurements [6]. Fingo Wu et al. have modified the FDTD electromagnetic computing method using LSTM neural networks, providing a reference for the application of neural networks in the electromagnetic forward problem in the time domain [7]. Other forms of neural networks, such as weakly supervised attention mechanisms [8], convolutional neural networks [9,10], and non-local computing neural networks [11] also find specific applications in electromagnetic computing.

Considering the capability of neural networks to improve forward and backward scatter calculations, Zhang Xu et al. constructed the EM-FCNN network, utilizing hyperparameters to control the surface roughness of the model and achieve high-speed scattering field calculations [12]. In terms of computing RCS using artificial neural networks, Rui Weng et al. implemented a computational model for the RCS of a deformed S-shaped cavity using artificial neural networks [13]. These studies demonstrate the significant potential of neural network applications in accelerating electromagnetic simulation calculations [14,18–22].

3. Research Ideas and Processes

3.1. Research Ideas

A comparison was conducted to evaluate the training time and computational accuracy of neural networks with different structures, utilizing a dataset containing grid data of ship scaling models and their corresponding RCS values. The training was performed in a data-driven manner using neural networks that incorporated LSTM neurons and general FCNN. The ability of neural networks to learn is affected by several factors, such as the learning rate, types of neurons, number of hidden layers and neurons, and the applied activation function. The aim was to determine the optimal neural network configuration for computing RCS values for scaling models of electric large-sized ships. The time spent on training the different neural network models, as well as the calculation speed and error percentage of the RCS values of the target objects after training, were compared.

3.2. Mathematical Model of LSTM Neural Networks

LSTM is a type of recurrent neural network that incorporates the structure of the forgetting gate, output gate, and input gate in its neurons, as Figure 1 shows. By introducing memory units, it effectively avoids issues such as gradient disappearance or gradient explosion that are often encountered in simple recurrent neural networks when processing time series data [23,24]. In comparison to general-purpose FCNN, LSTM demonstrates superior processing capabilities specifically tailored for time series data. In the optimization process employed in this study, the mesh data of the large-sized electric target being optimized change with each optimization step, thus forming a set of time series data that evolves over time. The details of parameters of equations show in the next Table 1.

$$\begin{cases} F_t = \sigma\left(W_f[H_{t-1}, x_t] + b_f\right) \\ I_t = \sigma(W_i[H_{t-1}, x_t] + b_i) \\ O_t = \sigma(W_o[H_{t-1}, x_t] + b_o) \\ \widetilde{C}_t = \tanh(W_o[h_{t-1}, x_t] + b_o) \\ C_t = F_t C_{t-1} + \widetilde{C}_t \\ H_t = O_t \tanh(C_t) \end{cases} \tag{1}$$

$$x_t = X_t + H_{t-1} \tag{2}$$

$$O_t = y_t + H_t \tag{3}$$

Table 1. The details of parameters of equations.

Parameter	Function
σ	activate function
W_f	weights matrix for forget
W_i	weights matrix for input
W_o	weights matrix for output
b_f	bias factor matrix for forget

Table 1. *Cont.*

Parameter	Function
b_i	bias factor matrix for input
b_o	bias factor matrix for output
x_t	the input layer state at the moment t
H_t	the hidden layer state at the moment t
C_t	the memory cell state at the moment t
X_t	electrical large-sized target mesh data input at the moment t
y_t	RCS value for electrically large-sized target

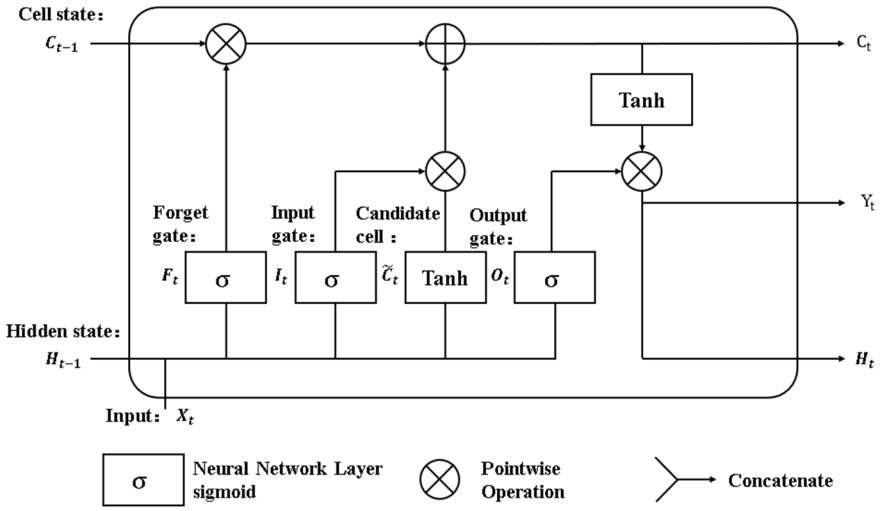

Figure 1. The work theory of neurons in LSTM neural networks.

In this paper, the LSTM neural network is utilized. The input layer state is determined by the current neural network tensor input X_t and the hidden layer state at the previous moment $t-1$. Similarly, the output layer state is determined by the memory unit at the current moment and the neural network tensor input at the current moment. The memory unit update is determined by the current neural network tensor input and the memory cell state at the previous moment. Due to the complexity of the grid data for the electrically large-sized target analyzed in this paper, it is crucial to update the memory unit at regular intervals to prevent the loss of significant information. Hence, when processing the time series sequence in this study, it is necessary to select a single input tensor with a sufficiently small time step.

The LSTM neural network is controlled by the gating mechanism, and the forgetting gate f_t determines how many data features need to be forgotten in the memory cell state C_{t-1} of the previous time node. The input gate i_t regulates the amount of information that can be stored regarding the data characteristics of the memory cell candidate state $\widetilde{C}_t$ at the current time step. The output gate o_t controls how many data features of the memory cell state C_t need to be output to the hidden layer state h_t at the current time node. Through the joint action of three gating units, the LSTM network can establish a data feature dependence in a long time series range, which has obvious advantages for the processing of long time series data.

3.3. Based on Data-Driven EM-LSTMNN Establishment

In the process of optimizing the RCS of electrically large-sized targets to minimize their radar detectability, numerous small-scale adjustments to the target's shape are necessary. These adjustments are recorded as elements in a dataset that contains both the mesh data for the targets and the corresponding RCS values. Each element in this sequence consists of three-dimensional mesh data and a long time series of RCS values for a large-sized target.

Specifically, the mesh data of the electrically large target used in a calculation is stored as a three-dimensional array, serving as an individual element within the dataset. Each time the mesh data are modified, the resulting new grid data are stored as the subsequent element in the dataset. In order to optimize the processing time and to account for the self-normalization characteristics of the chosen selu activation function, this study decides against normalizing the mesh data of the electrically large-sized target. The obtained time series of the target's mesh data is utilized as the input for the EM-LSTMNN, while the RCS value of the electrically large-sized target is set as the output. Subsequently, the EM-LSTMNN is trained through a data-driven approach.

3.4. Research Process

Using an electrically large-sized ship scale model as the calculated target object [18], adjustments were made to the superstructure of the model by moving the face vertex of the ship scaling model. This has resulted in a range of ship scale models that differ only in their top structures. It is important to ensure that no vertex of any facet component travels more than 10 mm from the corresponding point on the original model. The selected target model to be optimized is shown in the following Figure 2.

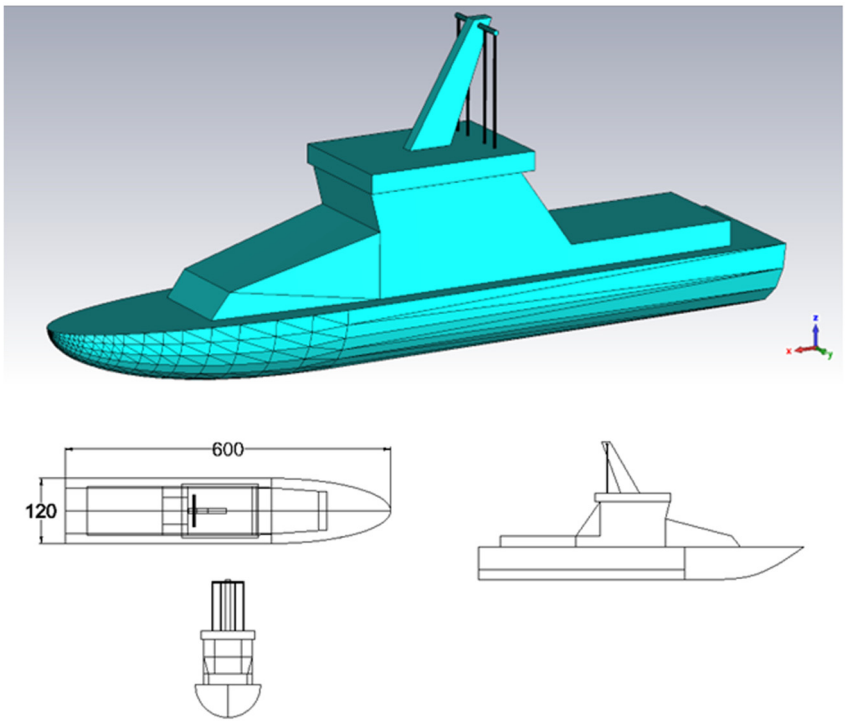

Figure 2. The scaled model and three views of the electric large-sized ship to be optimized. Units in the picture is mm.

The dataset utilized in this paper comprises two components: the mesh data of the electric large-size target scaling model as input values and the corresponding RCS values as label values. The RCS values were obtained using the traditional electromagnetic simulation calculation method for the ship scaling model, forming the dataset.

In this study, the simulation conditions involved calculating the RCS value at a fixed frequency point of 12 GHz for a pitch angle of 0° and azimuth angles ranging from 0° to 360° with a step size of 1°. The resulting RCS value at each time step is a one-dimensional vector consisting of 360 values. This vector is stored as the label value in the dataset. Simultaneously, the corresponding grid data are stored as the input data. For each subsequent time step, the mesh of the ship model's superstructure is modified, resulting in new mesh data and a new RCS label value obtained through simulation calculation. The grid data and RCS values for each new time step are added to the dataset.

It is important to note that the ship model's mesh data can only be adjusted once per time step, meaning that each modification to the mesh data represents a new time step. By accumulating data throughout the optimization process, a time-varying time series is constructed, with grid data serving as elements of the series. The next Table 2 shows the detail of the dataset.

Table 2. The details of the datasets.

Details of Dataset	Value
Numbers of grid data in dataset	400
Length of an RCS vector in dataset	360
Dataset cost memory	16,230 KB

This study establishes an LSTM neural network to compute RCS values for large electrical target models during electromagnetic scattering design optimization. After being trained with data and compared to both the FCNN and threshold recurrent neural network under identical conditions, it can be confirmed that the LSTM neural network is better suited for calculating RCS values in the low RCS optimization process of the electric large-size model than the typical FCNN.

The LSTM neural network addresses the limitations of the FCNN by enhancing its processing capability for time series data. By incorporating the LSTM architecture into the hidden layer structure of the FCNN, the improved neural network structure demonstrates an enhanced processing ability for long time series data. Additionally, it achieves higher computational accuracy and reduces training time in the design process of low-RCS optimization for electric large-sized targets.

The grid data of the ship scaling model and its corresponding RCS value are used to train the constructed neural network with the data-driven neural network.

By comparing the computational power and training time of the EM-LSTMNN with the general FCNN and the simpler gate recurrent unit (GRU) network, it has been verified that the EM-LSTMNN structure provides better acceleration in the low-RCS optimization process for electrically large-sized targets.

The EM-LSTMNN leverages its memory units and enhanced time series data processing capability to achieve faster computation and improved optimization results. In contrast, the general FCNN and the simpler GRU network lack the memory units and specialized mechanisms for handling time-dependent data, which limit their performance and efficiency in the low-RCS optimization process for electrically large-sized targets.

Therefore, the EM-LSTMNN stands out as the preferred choice due to its ability to achieve faster acceleration and superior performance in the optimization process, surpassing the general FCNN and the simpler GRU network in this context.

3.5. Comparison of Neural Network Computing Power of Different Structures

The dataset acquired during the low-RCS optimization process of the selected electric large-size target in this study is divided into 400 elements and arranged in chronological order to create the training set. For comparison purposes, the LSTM neural network, FCNN, and GRU are selected, and data-driven training is performed using the aforementioned training set. The results of the comparison are presented in the Table 3 below.

Table 3. Comparison of training results of the optimal structure of three neural networks.

The Type of Neural Network	Loss	Cost Time (s)
GRU	10.01895332	146.0487256
LSTM	8.144788742	105.9673052
FCNN	9.949327469	105.3547854
EM-FCNN	12.1204	519.0594008

The chosen loss function is the mean absolute percentage error (MAPE), which is utilized to prevent smaller data from being overshadowed when calculating the mean squared error for multi-output data. The table clearly shows that the FCNN has the quickest training speed, completing training in less time compared to the other two recurrent neural networks. On the contrary, the LSTM neural network outperforms the others in terms of overall performance, as it has the lowest loss function value and requires less training time.

In contrast to the EM-FCNN of its predecessor, Ref. [12] is used, then trained using the dataset used in this article. It can be seen that EM-FCNN consumes 519 s of time when training due to its large number of neurons and the activation function of relu, but the loss value is 12.1204, which is greater than the EM-LSTMNN used in this paper. This shows that the performance improvement of EM-LSTMNN compared to EM-FCNN proposed in this paper is obvious.

The computational capability of the LSTM neural network, after data-driven training on the RCS values of the selected electrically large-sized model, is illustrated in the Figure 3 below. It showcases the ability of the LSTM neural network to calculate the maximum error of the RCS value for the electrically large-sized model, ensuring it remains below 1 dB.

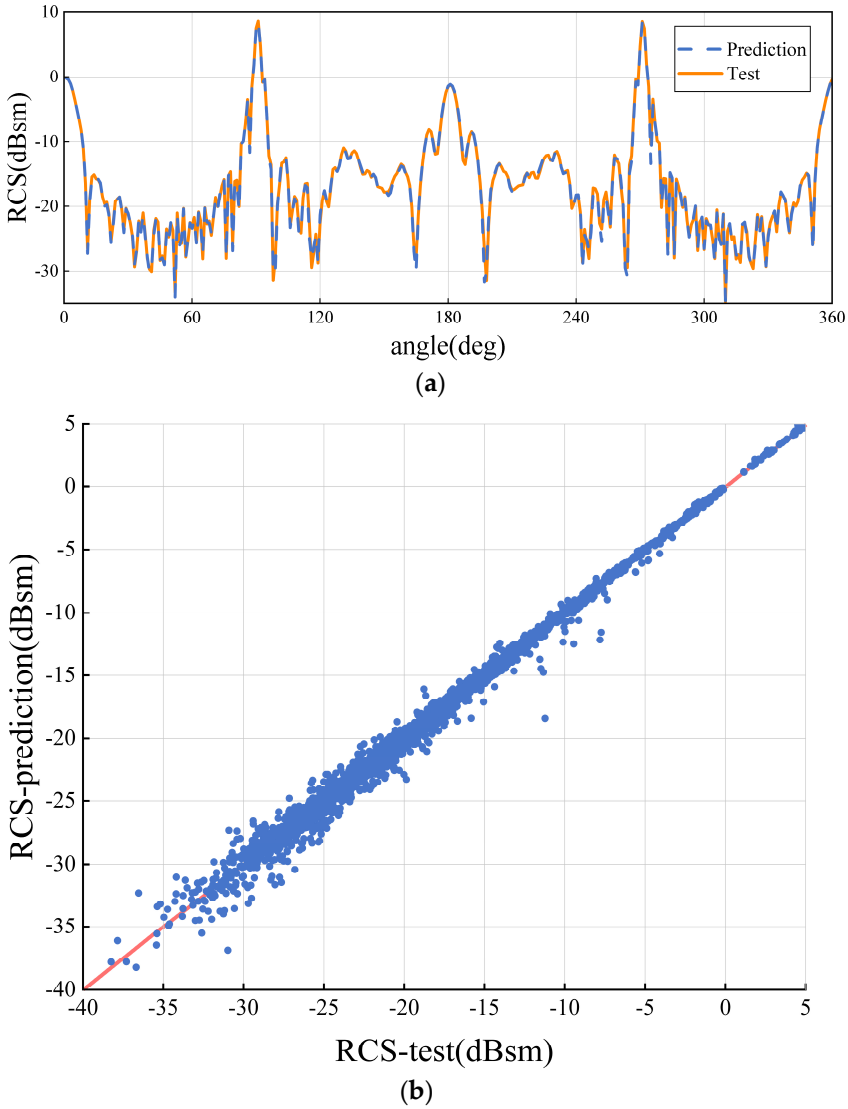

Figure 3. Comparison chart of RCS value calculation and electromagnetic simulation calculation results of electric large-sized model by LSTM network. (**a**) Comparison of the calculation results of pitch angle 0°, azimuth angle 0–360°, step size of 1°; (**b**) comparison of results with pitch angle 0°.

Three neural networks used to improve the electromagnetic simulation calculation process for the RCS value calculation accuracy of the electric large-sized model selected in this paper are shown in the Figure 4a below.

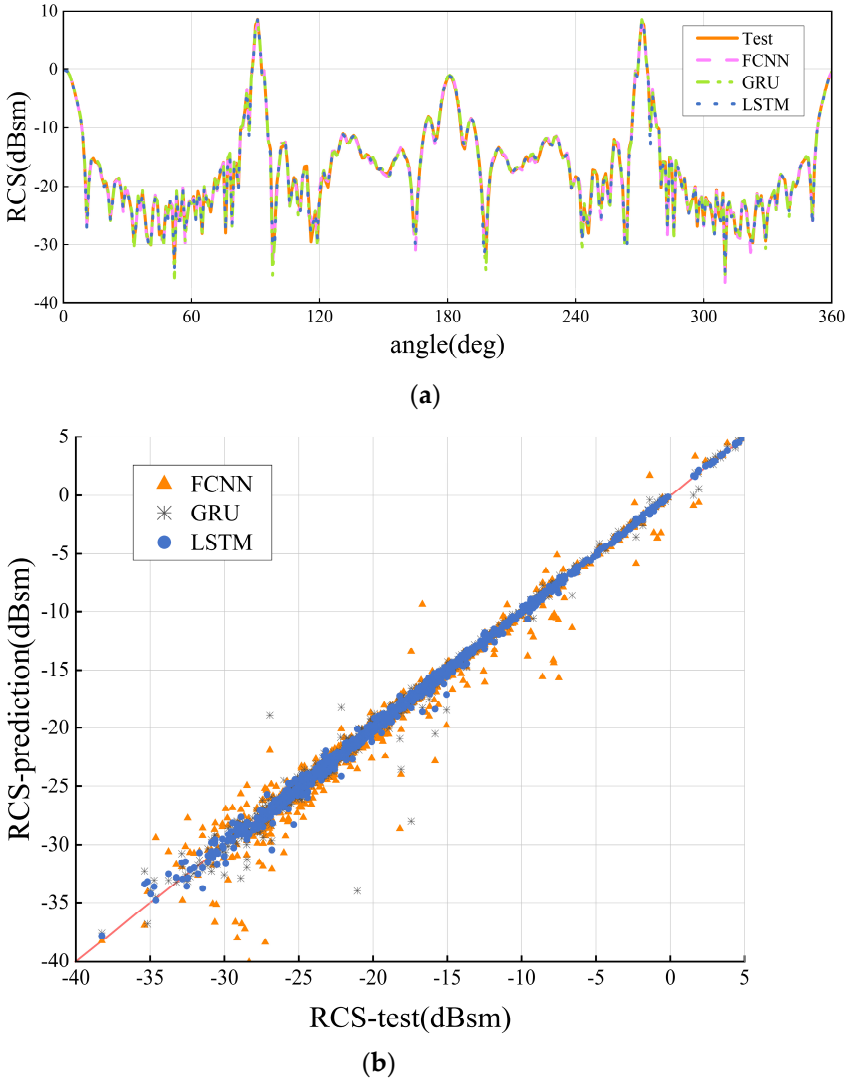

Figure 4. The calculation results of the RCS value of the electric large-sized model of the three neural networks are compared with the calculation results of electromagnetic simulation. (**a**) Comparison of the calculation results of pitch angle 0°, azimuth 0–360°, step size of 1°; (**b**) comparison of results with pitch angle 0°.

As depicted in Figure 4a above, both the FCNN and the GRU exhibit significant errors at certain azimuth angles. Additionally, Figure 4b demonstrates that although the FCNN achieves a small loss function, it fails to ensure precise calculations across the entire azimuth range. Particularly, a noticeable deviation occurs at an azimuth angle of 90°. In contrast, the LSTM neural network, with a small maximum error, demonstrates superior calculation performance in practical applications. Consequently, it can be concluded that employing the LSTM network in the low RCS optimization design process for the selected large-scale model enhances electromagnetic calculations, ensuring high computational accuracy while minimizing training time.

By employing neural networks with different structures to calculate the RCS value of the scaled-down target representing the electrically large-sized ship, it becomes evident that the LSTM network possesses a distinct advantage in processing long time series data through its memory units. This advantage significantly strengthens the RCS value

calculation capability of the electrically large-sized target during the optimization process, surpassing the other two neural networks.

3.6. Optimization of the EM-LSTMNN Structure

The learning rate, activation function, number of hidden layers, and number of neurons in EM-LSTMNN have varying impacts on the performance of neural networks. This paper explores the utilization of the self-normalization feature of the selu activation function during training to reduce the data processing time. Specifically, the exclusion of normalizing the mesh data of electrically large targets when constructing time series is proposed.

In order to obtain the EM-LSTMNN with a low training time and the highest computational accuracy, this paper uses grid search to optimize the EM-LSTMNN to find the number of hidden layers and learning rate that are most suitable for the usage scenario of this paper. By comparing four different activation functions, the self-normalization characteristics of selu when processing unnormalized data are verified. In this paper, the training effect of the selu activation function is significantly better than that of relu, LeakyReLU, and elu. Among the four activation functions, the most commonly used relu activation function has the worst training effect because it does not have the ability to process data with negative values of the independent variable x [25]. LeakyReLU is activated in negative regions in a better way than relu, the activation method used by $x = \alpha x$. Here, elu in the negative region is $x = e^x - 1$ and is superior to LeakyReLU in preventing gradient disappearance because the output value will tend to -1. Moreover, selu is a variant of elu that is activated in the negative value region by achieving self-normalization by changing the value [26], which has the best training effect.

In order to ensure the uniqueness of variables, the variable control method of single-variable experiments is used, and only one of the hidden layers of the neural network, the number of hidden layer neurons of the neural network, the activation function of the neural network, and the learning rate of the neural network is changed each time, and the structure of the EM-LSTMNN is optimized through grid search.

The learning rate of the control EM-LSTMNN is 0.0001, and the training result of the neural network is shown in the figure below.

As illustrated in Figure 5a, the activation function chosen for the LSTM network is LeakyReLU, with a learning rate of 0.0001. Both relu and elu exhibit similar trends in the loss function, but they yield significantly higher loss values compared to when selu is used as the activation function. When selu is employed as the activation function, the loss function value is influenced by the number of hidden layers and the number of neurons in the hidden layer of the neural network as follows: when the number of neurons in the hidden layer is fixed, increasing the number of hidden layers in the neural network leads to an increase in the number of neurons within each layer, while fixing the number of hidden layers and increasing the number of neurons in the hidden layer results in a decrease in the number of neurons.

It can be observed from Figure 5b that the training time of the LSTM network increases with the total number of neurons in the neural network, using a learning rate of 0.0001 across the four activation functions. In other words, having more layers in the hidden layer and a higher number of neurons within each layer can lead to an increased training time of the neural network. Consequently, the model that yields the best RCS calculation effect for large-scale electrical models in the LSTM network, under a learning rate of 0.0001, is a model comprising 3 layers of hidden layers and 512 neurons per layer, with selu as the activation function. This model exhibits a slight increase in training time in exchange for a significant decrease in the loss function value, while also demonstrating superior computational power.

When the change learning rate is 0.0003, the training results of the EM-LSTMNN are shown in the figure below.

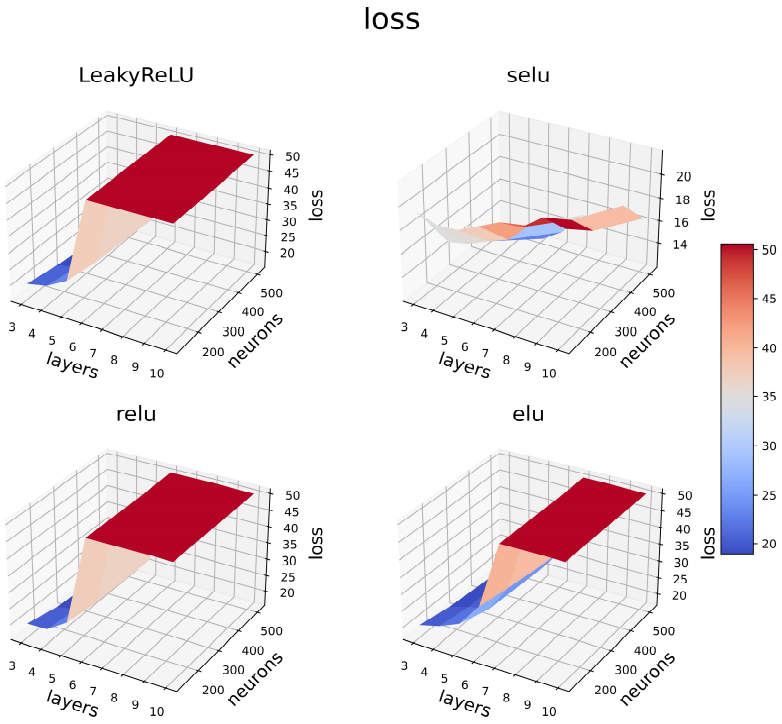

(**a**)

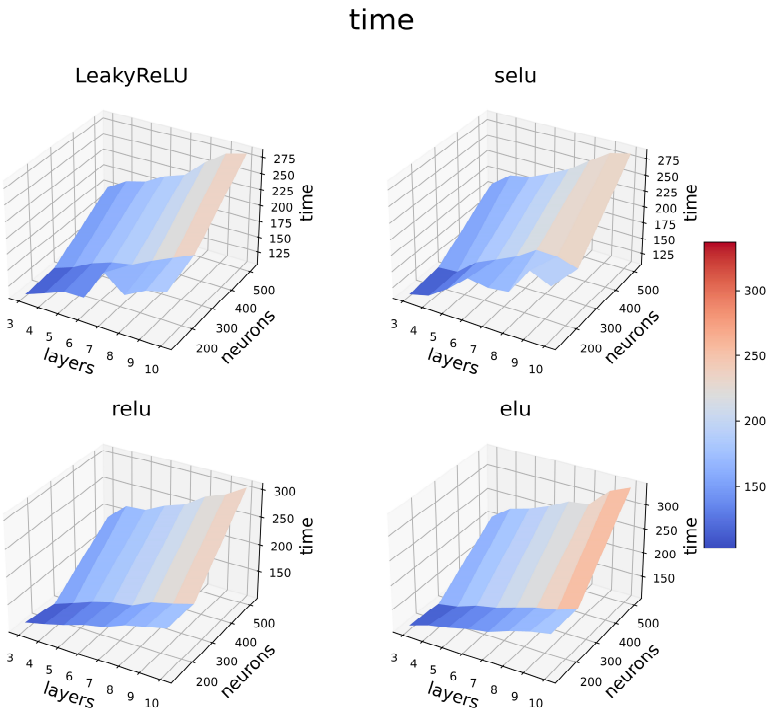

(**b**)

Figure 5. Comparison of loss function value and training time of EM-LSTMNN under the condition of a learning rate of 0.0001. (**a**) Comparison of loss function values; (**b**) comparison of training time required.

After carefully analyzing Figure 6, it is indeed challenging to discern a clear distinction in the impact of learning rates between 0.0001 and 0.0003. However, what becomes apparent is that abnormal training times occur exclusively when relu is employed as the activation function. Conversely, increasing the number of neurons and hidden layers

contributes to a reduction in training time. Nonetheless, it is important to note that even with these adjustments, the loss function values remain significantly higher compared to those obtained when selu is used as the activation function. Consequently, these outcomes do not align with the expected optimization direction outlined in this paper. Therefore, relu is not selected as the activation function for the optimal model of the EM-LSTMNN.

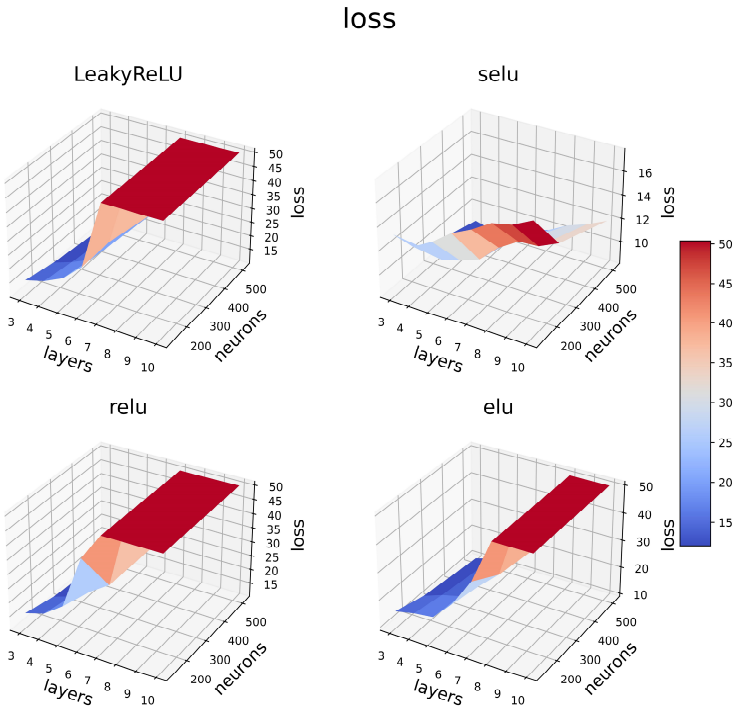

(**a**)

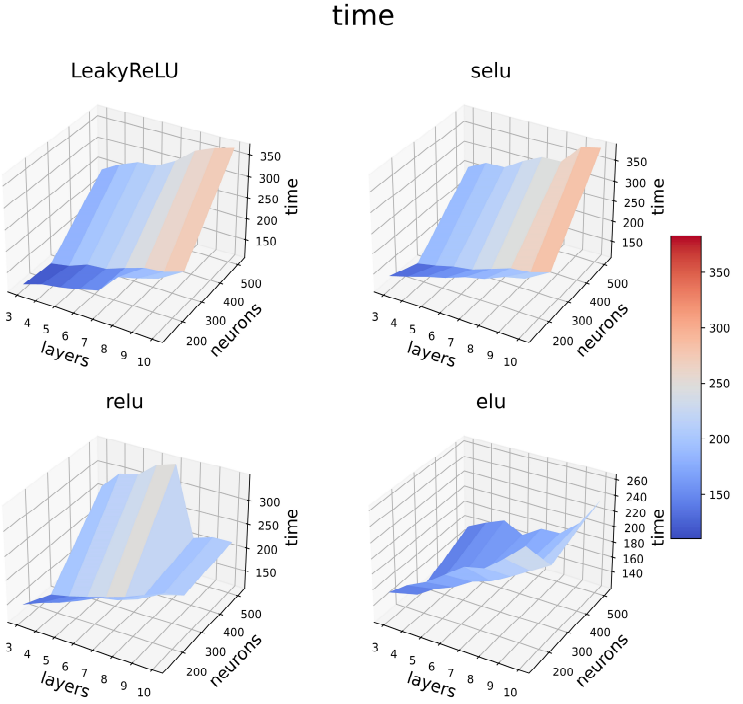

(**b**)

Figure 6. Comparison of loss function value and training time of EM-LSTMNN under the condition of a learning rate of 0.0003. (**a**) Comparison of loss function values; (**b**) comparison of training time required.

When the learning rate is increased to 0.0005, the training results of the EM-LSTMNN are shown in the figure below.

The impact of learning rate on the performance of the LSTM network, as depicted in Figure 7, is evident. When comparing the scenarios with learning rates of 0.0001 and 0.0003, this observation reveals that increasing the learning rate significantly reduces both the network's training time and the minimum value of the loss function. Thus, improving the learning rate becomes a crucial factor in calculating the RCS value for electrically large-sized targets using the LSTM network.

However, it is important to note that excessively increasing the learning rate may lead to unstable convergence of the neural network during training. Thus, it is suggested to identify the optimal model parameters for the LSTM network. This includes utilizing a learning rate of 0.0005, employing selu as the activation function, selecting three hidden layers, and configuring each hidden layer with 512 neurons. These settings yield the smallest loss function value and a shorter training time for the LSTM network. It is essential to avoid further increasing the learning rate, as it may hinder effective network training, preventing the loss function from reaching the desired precision within a limited number of training iterations.

The training results of the LSTM neural network under different learning rates have been sorted based on the loss function value in ascending order. The Table 4 below presents the data for ten groups of optimal solutions.

Based on the Table 5, the EM-LSTMNN architecture employed in this study clearly demonstrates promising features for training based on data and achieves a high level of computational accuracy. The network architecture consists of three hidden layers, each consisting of 512 neurons. The network uses the selu activation function and a learning rate of 0.0005 is used. These parameters contribute towards the network's ease of training and its ability to achieve consistent and reliable results.

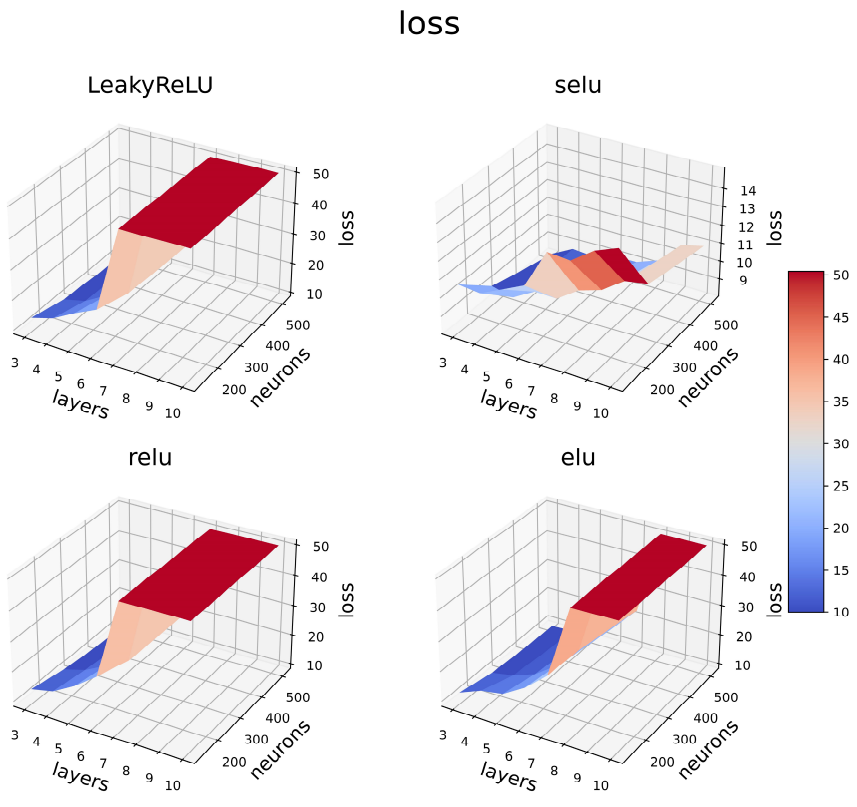

(**a**)

Figure 7. *Cont.*

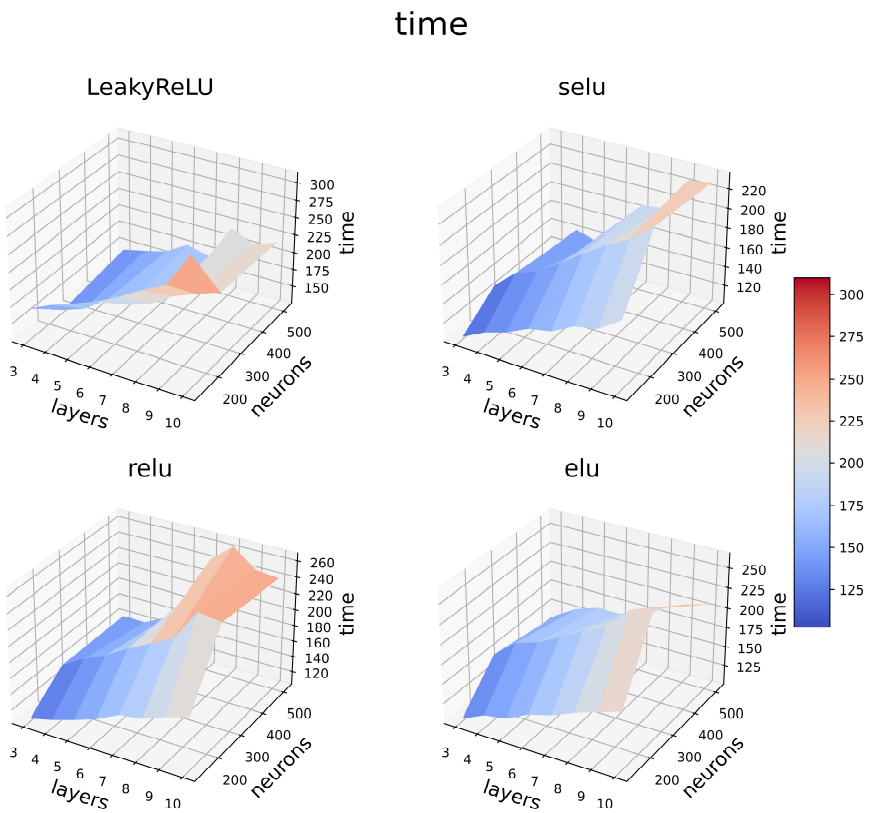

(**b**)

Figure 7. Comparison of loss function value and training time of EM-LSTMNN under the condition of a learning rate of 0.0005. (**a**) Comparison of loss function values; (**b**) comparison of training time required.

Table 4. Ten sets of EM-LSTMNN that are better solutions.

Activate Function	The Layers' Number of Hidden Layers	Number of Neurons in Hidden Layers	Learning Rate	Loss	Cost Time(s)
selu	3	512	0.0005	8.144788742	105.9673052
selu	4	512	0.0003	8.255619049	274.136621
selu	5	512	0.0003	8.497451782	275.3871346
selu	3	512	0.0003	8.666195869	250.6216426
selu	5	512	0.0005	8.668212891	135.9637468
selu	4	512	0.0005	8.752684593	142.3942518
selu	4	256	0.0005	8.815683365	149.5341535
selu	6	512	0.0005	9.013358116	163.7959225
selu	7	512	0.0005	9.042029381	187.1927898
selu	3	512	0.0005	9.07631588	129.7901208

Table 5. The best parameters of EM-LSTMNN.

Parameters of EM-LSTMNN	Value
Numbers of hidden layers	3
Number of neurons in hidden layers	512
Activate function	selu
Learning rate	0.0005

4. Discussion

Based on the previous discussion, it is clear that the learning rate plays a crucial role in the training time of neural networks. Increasing the learning rate generally leads to a

decrease in training time. However, it is important to find a balance because excessively large learning rates can cause instability during training, resulting in difficulties in achieving convergence. This issue becomes particularly prominent when the learning rate exceeds 0.0005, except when using the selu activation function. Furthermore, when the number of hidden layers in the neural network exceeds 8 and non-selu activation functions are utilized, a problem arises with loss values. This can be attributed to the increased likelihood of gradient vanishing as the number of hidden layers increases. Therefore, it may not be appropriate to employ deep neural networks in all cases when constructing neural networks to solve the problem of calculating RCS values. For the data presented in Table 4, adjustments were made to the hyperparameters, including the number of hidden layers, the number of neurons in each hidden layer, the learning rate, and the activation function. The EM-LSTMNN model was then evaluated using these different hyperparameters and the loss values were sorted from low to high. From the analysis, it is evident that the selu activation function outperforms other activation functions under the conditions of the electric large-sized scaling model used in this research. The loss values for the other activation functions were found to be higher compared to the selu activation function, suggesting that the choice of activation function greatly influences the computational performance of the neural network. Additionally, it was observed that the top ten neural network models had no more than 7 hidden layers, indicating that excessive hidden layers may hinder convergence.

5. Conclusions

An electromagnetic computation acceleration method, referred to as EM-LSTMNN, is proposed in this study to enhance the optimization process speed for reducing the RCS of electrically large targets. The approach presented in this paper aims to enhance the optimization speed for a low RCS of the electrically large targets. It achieves this by utilizing an LSTM neural network to process the grid data of electrically large targets and generate RCS values. This method simplifies the simulation calculation process by leveraging neural networks, ultimately improving traditional electromagnetic simulation calculations through faster neural network computations. When comparing the approach applied in this study, EM-LSTMNN, with other methods such as EM-FCNN, which also employ neural networks to improve electromagnetic simulation calculations, shows a significant reduction in training time. Specifically, the training time is reduced from 519 s for EM-FCNN to 106 s for EM-LSTMNN. Experimental results demonstrate that the EM-LSTMNN achieves a maximum error of less than 1 dB and requires a shorter training time. These findings provide valuable insights for future efforts in accelerating RCS value calculations during the design optimization process for reducing RCS in electrically large targets.

Author Contributions: Conceptualization, Y.Y.; methodology, Y.Y.; software, Y.Y. and S.X.; validation, Y.Y. and Q.W.; investigation, Y.Y.; data curation, Y.Y.; writing—original draft preparation, Y.Y.; writing—review and editing, Y.Y. and C.F.; visualization, Q.W.; supervision, C.F.; project administration, C.F. and Y.Y. All authors have read and agreed to the published version of the manuscript.

Funding: This research received no external funding.

Data Availability Statement: The data are not publicly available due to privacy.

Conflicts of Interest: The authors declare no conflict of interest.

References

1. Guo, R.; Shan, T.; Song, X.; Li, M.; Yang, F.; Xu, S.; Abubakar, A. Physics Embedded Deep Neural Network for Solving Volume Integral Equation: 2-D Case. *IEEE Trans. Antennas Propag.* **2022**, *70*, 6135–6147. [CrossRef]
2. Wei, Z.; Chen, X. Physics-Inspired Convolutional Neural Network for Solving Full-Wave Inverse Scattering Problems. *IEEE Trans. Antennas Propag.* **2019**, *67*, 6138–6148. [CrossRef]
3. Qi, Y.; Yu, C.; Dai, X. Research on Radar Plot Classification Based on Fully Connected Neural Network. In Proceedings of the 2019 3rd International Conference on Electronic Information Technology and Computer Engineering (EITCE), Xiamen, China, 18–20 October 2019; pp. 698–703. [CrossRef]

4. Smith, J.W.; Furxhi, O.; Torlak, M. An FCNN-Based Super-Resolution Mmwave Radar Framework for Contactless Musical Instrument Interface. *IEEE Trans. Multimed.* **2022**, *24*, 2315–2328. [CrossRef]
5. Yao, H.M.; Jiang, L. Enhanced PML Based on the Long Short Term Memory Network for the FDTD Method. *IEEE Access* **2020**, *8*, 21028–21035. [CrossRef]
6. Sima, W.; Zhang, H.; Yang, M.; Li, X. Diagnosis of small-sample measured electromagnetic transients in power system using DRN-LSTM and data augmentation. *Int. J. Elect. Power Energy Syst.* **2022**, *137*, 107820. [CrossRef]
7. Wu, F.; Fan, M.; Liu, W.; Liang, B.; Zhou, Y. An Efficient Time-Domain Electromagnetic Algorithm Based on LSTM Neural Network. *IEEE Antennas Wirel. Propag. Lett.* **2021**, *20*, 1322–1326. [CrossRef]
8. Choe, J.; Lee, S.; Shim, H. Attention-Based Dropout Layer for Weakly Supervised Single Object Localization and Semantic Segmentation. *IEEE Trans. Pattern Anal. Mach. Intell.* **2021**, *43*, 4256–4271. [CrossRef] [PubMed]
9. Dong, X.; Zheng, L.; Ma, F.; Yang, Y.; Meng, D. Few-Example Object Detection with Model Communication. *IEEE Trans. Pattern Anal. Mach. Intell.* **2019**, *41*, 1641–1654. [CrossRef] [PubMed]
10. Sheng, H.; Yang, F.; Jiang, H.; Yang, G.; Wang, D.; Zhang, N. Statistical analysis of infrared thermogram for CNN-based electrical equipment identification methods. *Appl. Artif. Intell.* **2021**, *36*, 2004348.
11. Wang, X.; Girshick, R.; Gupta, A.; He, K. Non-local Neural Networks. In Proceedings of the 2018 IEEE/CVF Conference on Computer Vision and Pattern Recognition, Salt Lake City, UT, USA, 18–22 June 2018; pp. 7794–7803. [CrossRef]
12. Zhang, X.; Wan, J.; Liu, Z.; Xu, F. RCS Optimization of Surface Geometry with Physics Inspired Neural Networks. *IEEE J. Multiscale Multiphys. Comput. Tech.* **2022**, *7*, 126–134. [CrossRef]
13. Weng, R.; Sun, D.; Yang, W.; Chen, X.; Lu, W. Efficient Broadband Monostatic RCS Computation of Morphing S-Shape Cavity Using Artificial Neural Networks. *IEEE Antennas Wirel. Propag. Lett.* **2023**, *22*, 263–267. [CrossRef]
14. Collins, A.M.; O'Dea, A.; Brodie, K.L.; Bak, A.S.; Hesser, T.J.; Spore, N.J.; Farthing, M.W. Automated Extraction of a Depth-Defined Wave Runup Time Series from Lidar Data Using Deep Learning. *IEEE Trans. Geosci. Remote Sens.* **2023**, *61*, 5700913. [CrossRef]
15. Yuan, D.; Xie, X.; Gao, G.; Xiao, J. Advances in Hyperspectral Image Classification with a Bottleneck Attention Mechanism Based on 3D-FCNN Model and Imaging Spectrometer Sensor. *J. Sens.* **2022**, *2022*, 7587157. [CrossRef]
16. Wallentine, S.; Jost, R.J.; Reddy, C.J.; Cannon, J.M. RCS Simulations and Measurements of an Autonomous Spherical RCS Calibration Device. In Proceedings of the 2022 Antenna Measurement Techniques Association Symposium (AMTA), Denver, CO, USA, 9–14 October 2022; pp. 1–5. [CrossRef]
17. IHF-Boat. A Measurement Standard for Polarimetric RCS Imaging. Available online: https://www.ihf.rwth-aachen.de/en/research/research-topics/further-research-topics/rcs-measurements/ihf-boat (accessed on 7 September 2013).
18. Li, X.-Q.; Song, L.-K.; Bai, G.-C.; Li, D.-G. Physics-informed distributed modeling for CCF reliability evaluation of aeroengine rotor systems. *Int. J. Fatigue* **2023**, *167*, 107342. [CrossRef]
19. Li, X.-Q.; Song, L.-K.; Choy, Y.-S.; Bai, G.-C. Multivariate ensembles-based hierarchical linkage strategy for system reliability evaluation of aeroengine cooling blades. *Aerosp. Sci. Technol.* **2023**, *138*, 108325. [CrossRef]
20. Li, S.; Lai, S.-J.; Liu, J.; Wu, S.; Chen, L. A MLP Based FDTD Method. *J. Comput. Chem.* **2020**, *8*, 279–284. [CrossRef]
21. Pons, A.; Somolinos, Á.; González, I.; Cátedra, F. Fast Computation by MLFMM-FFT with NURBS in Large Volumetric Dielectric Structures. *Electronics* **2021**, *10*, 1560. [CrossRef]
22. Massa, A.; Marcantonio, D.; Chen, X.; Li, M.; Salucci, M. DNNs as Applied to Electromagnetics, Antennas, and Propagation—A Review. *IEEE Antennas Wirel. Propag. Lett.* **2019**, *18*, 2225–2229. [CrossRef]
23. Ioffe, S.; Szegedy, C. Batch Normalization: Accelerating Deep Network Training by Reducing Internal Covariate Shift. In Proceedings of the 32nd International Conference on Machine Learning, Lille, France, 6–11 July 2015.
24. Ma, L.; Hu, C.; Cheng, F. State of Charge and State of Energy Estimation for Lithium-Ion Batteries Based on a Long Short-Term Memory Neural Network. *J. Energy Storage* **2021**, *37*, 102440. [CrossRef]
25. Kaloev, M.; Krastev, G. Comparative Analysis of Activation Functions Used in the Hidden Layers of Deep Neural Networks. In Proceedings of the 2021 3rd International Congress on Human-Computer Interaction, Optimization and Robotic Applications (HORA), Ankara, Turkey, 11–13 June 2021; pp. 1–5. [CrossRef]
26. Stursa, D.; Dolezel, P. Comparison of ReLU and linear saturated activation functions in neural network for universal approximation. In Proceedings of the 2019 22nd International Conference on Process Control (PC19), Strbske Pleso, Slovakia, 11–14 June 2019; pp. 146–151. [CrossRef]

Disclaimer/Publisher's Note: The statements, opinions and data contained in all publications are solely those of the individual author(s) and contributor(s) and not of MDPI and/or the editor(s). MDPI and/or the editor(s) disclaim responsibility for any injury to people or property resulting from any ideas, methods, instructions or products referred to in the content.